RESEARCH ARTICLE

East Asian summer precipitation in AWI-CM3: Comparison with observations and CMIP6 models

Jian Shi[1,2] 🟢 | **Christian Stepanek**[1] | **Dmitry Sein**[1] | **Jan Streffing**[1,3] | **Gerrit Lohmann**[1,4]

[1]Alfred Wegener Institute, Helmholtz Centre for Polar and Marine Research, Bremerhaven, Germany

[2]Key Laboratory of Meteorological Disaster, Ministry of Education/ Collaborative Innovation Center on Forecast and Evaluation of Meteorological Disasters, Nanjing University of Information Science and Technology, Nanjing, China

[3]Jacobs University Bremen, Bremen, Germany

[4]University of Bremen, Bremen, Germany

Correspondence
Jian Shi, Alfred Wegener Institute, Helmholtz Centre for Polar and Marine Research, Bremerhaven, Germany.
Email: jian.shi@awi.de

Abstract

Owing to the complicated spatial–temporal characteristics of East Asian precipitation (EAP), climate models have limited skills in simulating the modern Asian climate. This consequently leads to large uncertainties in simulations of the past EAP variation and future projections. Here, we explore the performance of the newly developed Alfred Wegener Institute Climate Model, version 3 (AWI-CM3) in simulating the climatological summer EAP. To test whether the model's skill depends on its atmosphere resolution, we design two AWI-CM3 simulations with different horizontal resolutions. The result shows that both simulations have acceptable performance in simulating the summer mean EAP, generally better than the majority of individual models participating in the Coupled Model Intercomparison Project (CMIP6). However, for the monthly EAP from June to August, AWI-CM3 exhibits a decayed skill, which is due to the subseasonal movement of the western Pacific subtropical high bias. The higher-resolution AWI-CM3 simulation shows an overall improvement relative to the one performed at a relatively lower resolution in all aspects taken into account regarding the EAP. We conclude that AWI-CM3 is a suitable tool for exploring the EAP for the observational period. Having verified the model's skill for modern climate, we suggest employing the AWI-CM3, especially with high atmosphere resolution, both for applications in paleoclimate studies and future projections.

KEYWORDS
AWI-CM3, CMIP6, East Asia, summer precipitation

1 | INTRODUCTION

East Asian summer monsoon (EASM) is the dominant atmospheric circulation over East Asia during boreal summertime, which brings abundant moisture from the tropical–subtropical ocean and contributes 40%–50% (60%–70%) of the total precipitation in south (north) China annually (Lei et al., 2011). Given its importance to local hydroclimate and livelihood of billions of people, enormous efforts were made to investigate the EASM and

accompanied East Asian precipitation (EAP) variations across timescales. For example, the EASM underwent a decadal shift since the late 1970s, leading to increased floods and droughts in south and north China, respectively. However, whether this decadal variation is caused by anthropogenic forcings (Lin et al., 2016; Tian et al., 2018; Wang et al., 2013; Zhu et al., 2012) or is due to variability inherent to the climate system (Fu et al., 2009; Li et al., 2010; Yu et al., 2015) remains controversial. Climate models are becoming powerful tools to investigate the EASM/EAP behaviour and associated dynamics, especially for the past and future, where reliable observations are limited or unavailable. For example, modelling studies indicated that EAP increased at the middle Holocene, qualitatively consistent with the proxies, in response to enhanced orbital-forced insolation and vegetation feedbacks (Chen et al., 2021; Piao et al., 2020; Tian & Jiang, 2013; Zheng et al., 2013). In addition, climate models project an overall increase in the summer precipitation in a future warmer world, caused by the warming-induced increase in the atmospheric moisture content (Chen & Sun, 2013; Li et al., 2019; Seo et al., 2013; Zhou et al., 2018).

An important presupposition of using climate models to investigate the EAP is that these models should have an acceptable ability to reproduce the observations, which is determined by the models' reasonable responses to internal and external forcings. Although the model performance during the instrumental period does not guarantee its performance for future or past climate changes, better reproduction of a climate model potentially implies more accurate physical processes or more reasonable parameterizations concerning the climate system, which is favourable to the better future or past climate simulations. However, owing to the complicated spatial–temporal characteristics of EAP and model limitations, climate models have limited skills in simulating the modern Asian climate (Huang et al., 2013; Song & Zhou, 2014). This consequently leads to significant uncertainties in simulations of EAP variation for past climates and future projections. For instance, climate models participating in the third phase of the Paleoclimate Modelling Intercomparison Project (PMIP3) simulated an overall increase in EAP at the middle Holocene (∼6000 years ago), while there is less consistency in the PMIP3 model ensemble regarding the precipitation increase over south China (Tian & Jiang, 2013; Zheng et al., 2013). Furthermore, the amplitude of summer EAP increases at the end of the 21st century shows large intermodel differences among the models participating in the Coupled Model Intercomparison Project (CMIP), and in iteration 5 of CMIP (CMIP5) the uncertainties mainly come from the model dependence of precipitation-related dynamic

processes (Zhou et al., 2018), related to the amplitude of projected warming (Li et al., 2019).

Therefore, it is necessary to evaluate the climate models against observations before using them to investigate present, past and future climate and its changes. The ensemble of multimodels (MME) reduces the inherent biases within individual models, hence emphasizing their common signal. It has been shown that the MME provides a more reliable reproduction of observations or reconstructions than most individual models (Feng et al., 2014; Haywood et al., 2020; Jiang et al., 2020; Xin et al., 2020). Previous studies indicated that the latest CMIP6 MME is more skilful than the former CMIP5 MME in the climatological precipitation over east China (Jiang et al., 2020; Xin et al., 2020). In addition, climate models with higher horizontal atmosphere resolution are considered to have a better capacity in simulating the summer EAP than the lower atmosphere resolution models, due to their more realistic description of orographic forcing, which is crucial to EAP formation (Ding et al., 2021; Gao et al., 2006, 2008; Yao et al., 2017). Jiang et al. (2016) analysed systematically the ability of climate models to simulate the East Asian monsoon. Their work implies that models' ability varies with season and is affected by their horizontal resolution to a certain degree and that the MME outperforms most individual models in every respect. Lohmann et al. (2021) emphasized that simulated mid-Holocene climate differences can be very sensitive to the model resolution and reproduction of orographic detail. Nevertheless, other studies augured that model resolution is not a determinant factor regarding the simulation of EAP (Xin et al., 2021).

Here, we employ the third generation of climate model developed at the Alfred Wegener Institute (AWI-CM3) introduced by Streffing et al. (2022) and evaluate its simulation of the climatological summer EAP for a modern climate state against observations and the ensemble of CMIP6 models. Streffing et al. (2022) has shown that, from the viewpoint of reproduction of observed global climatology, the AWI-CM3 has higher skill than the average of the models that participated in CMIP6. The influence of horizontal resolution was analysed for its atmosphere model on systematic errors, cloud radiative forcing and extratropical cyclone characteristics (Jung et al., 2006; Potter, 1995; Tibaldi et al., 1990). Key characteristics of extratropical cyclones, which are highly sensitive to model resolution, show a tendency to more realistic patterns with increased resolution. Here, we further use the AWI-CM3 model in a coupled atmosphere–ocean setting and in a more specific manner to explore the model's performance for simulating summer precipitation over East Asia considering different horizontal resolutions.

2 | MODEL, DATA AND METHODS

2.1 | AWI-CM3 and experiments design

The AWI-CM3 consists of two major components: the atmosphere module is the global Integrated Forecasting System (IFS) in the version OpenIFS (version 43R3V1; ECMWF, 2017a, 2017b, 2017c) developed at the European Centre for Medium-Range Weather Forecast, and the ocean module is the second version of the Alfred Wegener Institute's global ocean model, the Finite volumE Sea ice-Ocean Model (FESOM2) with unstructured meshes (Danilov et al., 2017). The OpenIFS has a superior computational efficiency owing to its semi-Lagrangian semi-implicit advection scheme, allowing for advection distances beyond the Courant–Friedrichs–Lewy condition, and is consequently numerically stable at much longer time steps than equivalent Eulerian integrations, which enables us to run high-resolution simulations with affordable computational resources (Streffing et al., 2022).

Two AWI-CM3 simulations that differ in spatial detail resolved in the atmosphere are exerted. The relatively lower-resolution simulation is performed at a truncation of TCo159 (~61 km) with 91 vertical layers for the OpenIFS, coupled with the FESOM2 using a middle high-resolution mesh (Sein et al., 2016), containing about 1.3 million surface grid nodes, which is denser over the eddy-resolving areas such as the Kuroshio and Gulf Stream regions (Figure S1, Supporting Information). This simulation is carried out for 83 years with constant forcing of the year 1990 and will be referred to as TCo159. The setup of the higher resolution simulation is identical to that of the TCo159 except it is performed at a truncation of TCo319 for the OpenIFS, leading to a higher spatial resolution (~31 km). This simulation is integrated for 90 years and will be referred to as TCo319. To improve the state of equilibrium of the modelled climates, the ocean was spun up for 100 years before starting the two simulations, while the atmosphere was not. Figure S2 indicates that both simulations have not reached full equilibrium due to the short spin-up and simulation time, resulting in a drift of annual global mean surface air temperature (GMSAT) especially for the first 30 years (linear trend of 0.32 and 0.16 K·decade^{-1} for the TCo159 and TCo319 simulation, respectively). In this study, the last 50 years of each simulation are analysed, where the strong initial model drift has reduced to a relatively small annual GMSAT linear trend of 0.06 and 0.03 K·decade^{-1} for the TCo159 and TCo319 resolution, respectively.

2.2 | Data and methods

In addition to our AWI-CM3 simulations, we consider output from other modelling groups. In the lack of a simulation with stable 1990 climate forcing in the CMIP6 protocol, we analyse the monthly outputs of the historical experiments of 53 CMIP6 models (Table S1). Results are compared with our AWI-CM3 simulations TCo159, TCo319 and observational data. Corresponding observed monthly precipitation is obtained from Asian Precipitation-Highly Resolved Observational Data Integration Towards Evaluation (APHRODITE) V1101 and V1101EX (Yatagai et al., 2009), which has a 0.25° horizontal resolution over monsoonal Asia. Besides, two sets of precipitation data are used: the Full Data Monthly Product of Global Precipitation Climatology Centre (GPCC_FD) v2022 (Schneider et al., 2022) and Climate Research Unit Time Series (CRU_TS) v4.05 (Harris et al., 2020) to evaluate the AWI-CM3 from a global perspective. Furthermore, the Japanese 55-year reanalysis (JRA-55; Kobayashi et al., 2015) and Hadley Centre Sea Ice and Sea Surface Temperature data set (HadISST; Rayner et al., 2003) are utilized to examine the precipitation-related atmospheric and oceanic pattern in climate models. All the modelled and observed precipitation data are interpolated to the 0.25° × 0.25° resolution using the bilinear interpolation for comparison. Other atmosphere and ocean data are interpolated to the 2° × 2° resolution. The period of 1958–2014 is selected for the comparison of observations and CMIP6 models with AWI-CM3. Information on simulations and observations is summarized in Table 1. We also show that the comparison result is insensitive to the observation dataset and periods selected (Figures S3 and S4).

The Taylor diagram (Taylor, 2001) illustrates a model's capacity in reproducing the observed pattern distribution and intensity of precipitation, respectively shown as the spatial correlation coefficient (SCC) in the angular coordinate and standardized deviation normalized by observation (NSD) in the radial coordinate. The skill score (SS) is further used to quantify model performance against observations, which is defined as

$$SS = \frac{4(1+SCC)}{\left(NSD + \frac{1}{NSD}\right)^2 (1+SCC_0)},$$

where SCC_0 is the maximum correlation attainable that is assumed as 1 (Taylor, 2001).

It is not rigorous to compare the AWI-CM3 simulations, observations and CMIP6 historical simulations. AWI-CM3 simulations presented here are designed

TABLE 1 Observations and simulations utilized in this study

Data	Resolution (lat × lon)	Available period	Analysis period	References
GPCC_FD v2022	0.25° × 0.25°	1891–2019	1958–2014	Schneider et al. (2022)
CRU_TS v4.05	0.5° × 0.5°	1901–present		Harris et al. (2020)
APHRODITE V1101/V1101EX	0.25° × 0.25°	1951–2015		Yatagai et al. (2009)
JRA-55	1.25° × 1.25°	1958–present		Kobayashi et al. (2015)
HadISST	1° × 1°	1870–present		Rayner et al. (2003)
CMIP6 Historical	~1.3° × 1.8°[a]	1850–2014		See Table S1
TCo159	~0.56° × 0.55°	83 years	Last 50 years	This study
TCo319	~0.28° × 0.28°	90 years		

[a]Average resolution of CMIP6 models.

towards a quasi-equilibrium state whereas the observations and CMIP6 historical simulations represent transient climates. However, since the AWI-CM3 simulations are based on Common Era 1990 forcings, their climatologies over the analysis period reach a 1990-like equilibrium state that falls into the period of observations and CMIP6 historical runs. Therefore, it is acceptable to compare the AWI-CM3 simulations with the observed climatology and with CMIP6 historical simulations during 1958–2014.

3 | GOOD PERFORMANCE OF SUMMER MEAN EAP IN AWI-CM3

3.1 | Evaluation of AWI-CM3 and CMIP6 models

We first give an overall evaluation of the climate models with regard to global land precipitation (Figure S4). Generally, the CMIP6 models show acceptable skill in capturing the observed boreal summer (June–July–August; JJA), boreal winter (December–January–February; DJF) and annual mean precipitation, with large spatial similarity and small standardized deviation bias. These two statistics are further improved in the CMIP6 ensemble mean, demonstrating the advantage of using the MME. Proceeding to our own model we find that the AWI-CM3 has an outstanding ability in reproducing observed global land precipitation, which is comparable with the MME of CMIP6. It is noted that the simulation at TCo319 resolution has an overall improvement of simulated characteristics of global average land precipitation in comparison to the TCo159 simulation in all considered seasons and for the annual mean. Both the AWI-CM3 and CMIP6 models exhibit weaker performance in simulating the JJA precipitation. During that season global land precipitation is concentrated in the monsoon areas of the

Northern Hemisphere, indicating a challenge for climate models in reproducing the monsoonal precipitation (Figures S3 and S5).

Climate models show a greater disparity in their capability in simulating the summer mean EAP than at the global scale. Generally, they show good skills in reproducing the spatial distribution of the observed summer averaged precipitation (Figure 1a). Most of the SCCs are larger than 0.7. However, simulated standard deviations are generally slightly smaller than that inherent to the observational data set. As a result, although the CMIP6 MME has superior performance than most individual members, it still underestimates the standardized deviation of local precipitation. In contrast, the AWI-CM3, employed at both TCo159 and TCo319 resolution, has a quite high SCC, which is greater than that of most CMIP6 models and close to their MME (Figure 1a). The NSD of AWI-CM3 also exhibits a similar bias as CMIP6 MME relative to the observation, although it overestimates the standardized deviation. In summary, the AWI-CM3 has an almost equivalent capacity to the CMIP6 MME in simulating climatological summer averaged EAP, and is hence at par with the best-performing individual CMIP6 models from the perspective of the skill score.

After comparing the AWI-CM3 and CMIP6 models' performance using the Taylor diagram, we further calculate the skill scores of individual models. We rank all the simulations and determine the relative skill and performance of AWI-CM3 among the state-of-the-art models (Figure 2a). It is clearly shown that for the summer averaged EAP, the AWI-CM3 with both TCo319 and TCo159 are superior to more than 80% of the individual 53 CMIP6 models, which show a performance close to the CMIP6 MME. Moreover, the higher atmosphere resolution of TCo319 (SS = 0.94) helps to slightly improve the simulation of summer mean EAP compared to TCo159 (SS = 0.92).
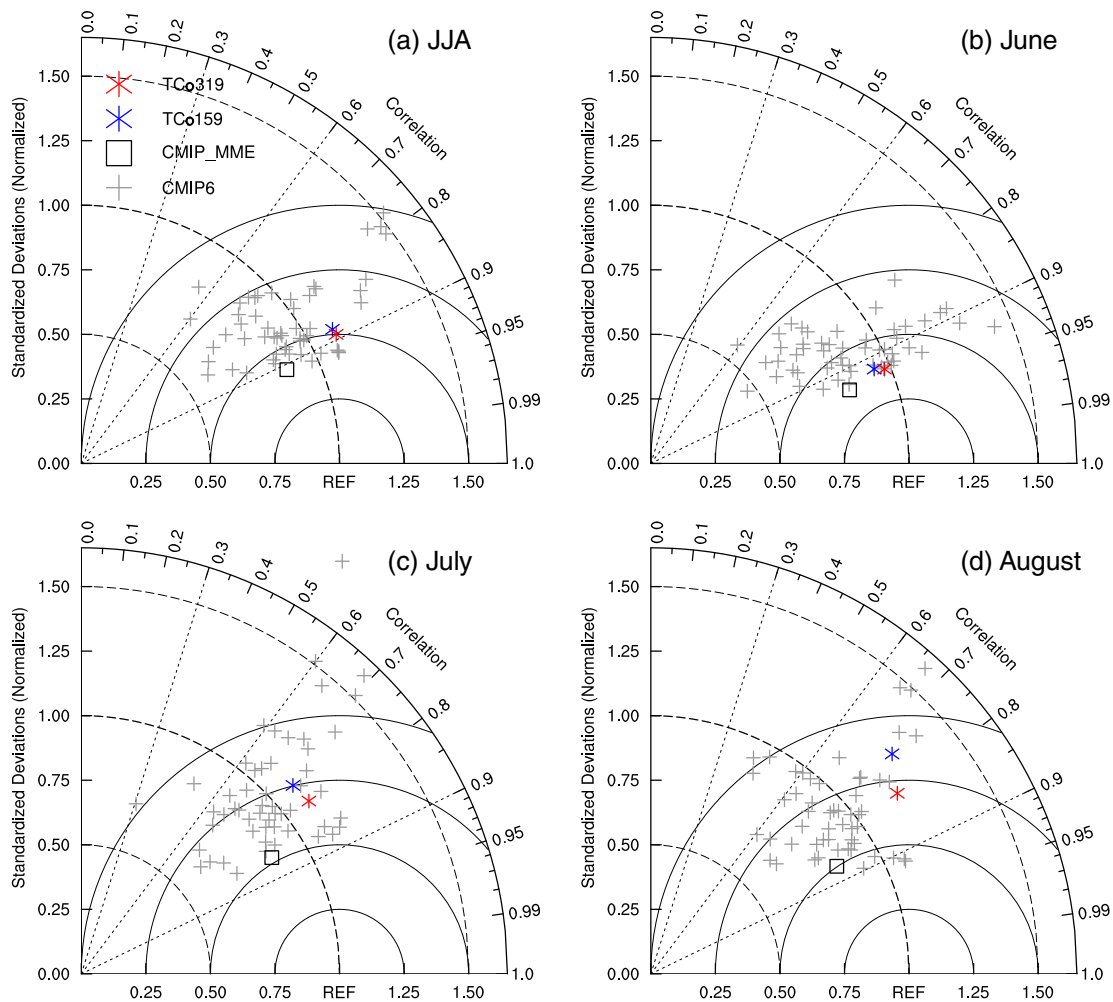
FIGURE 1　Taylor diagram displaying pattern statistics of East Asian (20°–50°N, 105°–145°E) land precipitation in AWI-CM3 at TCo159, TCo319 resolution and CMIP6 historical runs relative to APHRODITE [Colour figure can be viewed at wileyonlinelibrary.com]

The spatial patterns of observed and modelled precipitation show more details that are so far concealed in our skill score analysis. Summer precipitation concentrates over southeast China and south Japan, decaying from the coast to the inland region due to the moisture transported from adjacent oceans. In addition, there are several maxima related to local orography, such as Wuyi, Nanling and Taiwan Mountains (Figure 3; for geographical locations please refer to Figure S6). The general pattern shown by the observation is roughly reproduced by CMIP6 MME and AWI-CM3. However, due to the coarse orography applied in most CMIP6 models, these models and their ensemble fail to capture the precipitation centres over south China caused by the orographic lifting. Meanwhile, AWI-CM3, with a relatively high resolution of the orography, can simulate these precipitation centres at both TCo159 and TCo319 resolution, although their amplitude is inconsistent with observations (Figure 3).

In addition to evaluating the pattern distribution of simulated summer precipitation, we further investigate

the precipitation intensity in climate models. For the CMIP6 MME, the most conspicuous bias is over north China and Mongolia, where the modelled summer mean precipitation is overestimated by approximately 50% with respect to the observation (Figure 3). As a consequence, the northern boundary of EASM, the northernmost region that EASM moisture could reach, is also located in the north of the observed boundary, which implies large uncertainties using CMIP6 models to study the climate of the monsoon–semi-arid transition areas. Compared to the CMIP6 MME, AWI-CM3 with TCo159 and TCo319 resolution have much better performance in simulating the summer precipitation intensity, especially over the mid-latitude Asia, although with excessive precipitation near Taihang Mountain. Therefore, the northern boundary of EASM simulated by the AWI-CM3 is close to the observed boundary. For south China, both CMIP6 MME and AWI-CM3 show slightly more precipitation than observation. The precipitation bias pattern of AWI-CM3 with TCo319 is almost identical to TCo159, but has a
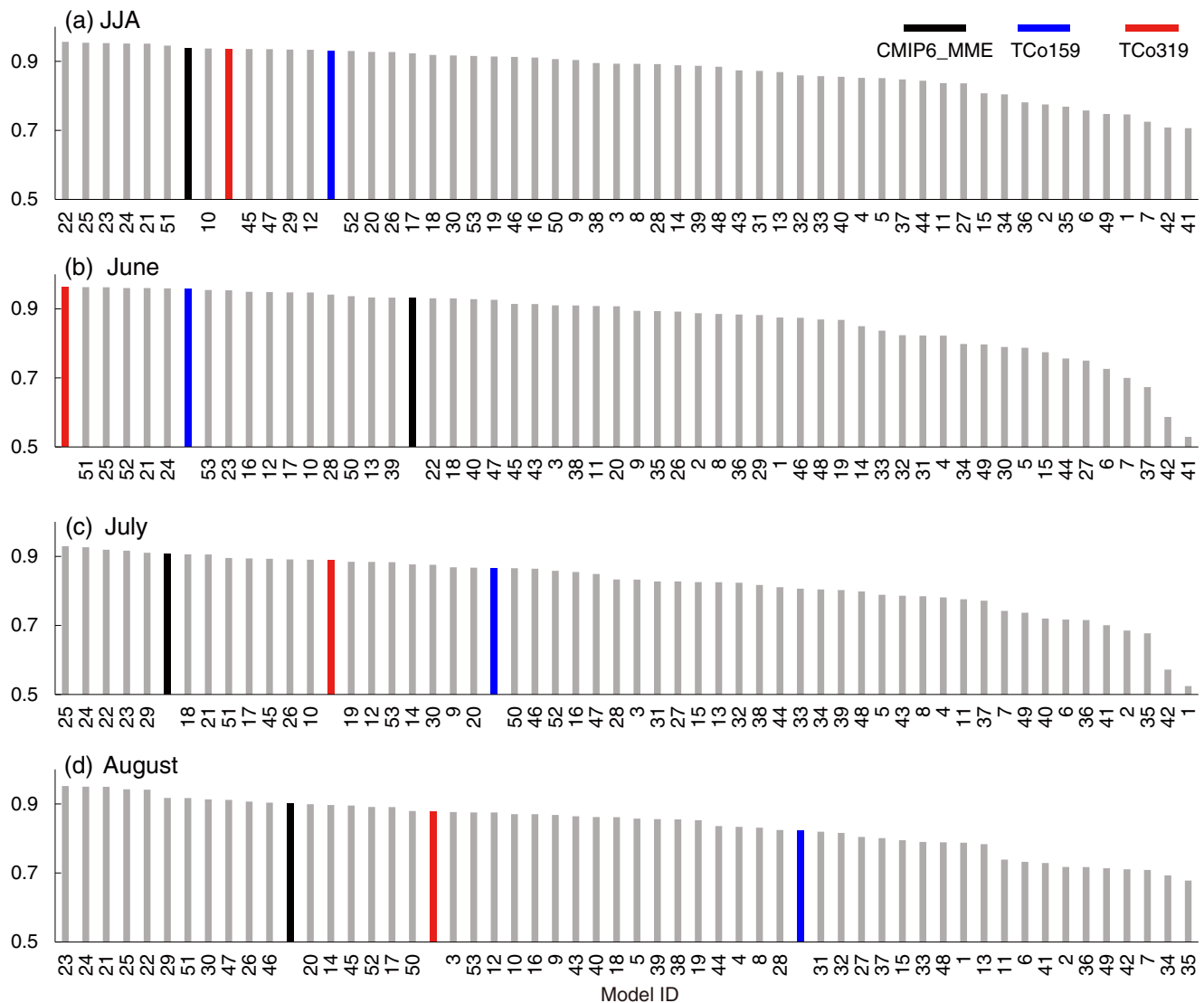
FIGURE 2 Skill scores of AWI-CM3 TCo159 (blue), TCo319 (red), CMIP6 historical runs (grey) and CMIP6 MME (black) in simulating East Asian (20°–50°N, 105°–145°E) precipitation relative to the APHRODITE precipitation for JJA mean (a) and individual summer months (b–d), ranked in order of descending skill. Please refer to Table S1 for the ID of a specific model [Colour figure can be viewed at wileyonlinelibrary.com]

smaller amplitude, indicating an improvement of model performance in simulating the summer mean EAP that may be attributed to increased spatial resolution of the atmosphere model in AWI-CM3.

3.2 | Causes of models' bias

The summer precipitation over East Asia is closely linked to the EASM, bringing warm and moist air from the western Pacific and Indian Ocean to the continent. Climatologically, the East Asian summer precipitation has two moisture sources: one is based on a coupling to the Southwest monsoon from India, the Bay of Bengal and

South China Sea; the other is linked to the southeast monsoon along with the western Pacific subtropical high (WPSH) (Figures 4a and 5). Strong moisture converges in the tropical region and encounters cold air from high latitudes, forming precipitation in East Asia. The CMIP6 MME simulates an anomalous cyclone and anticyclone over the subtropical and extratropical northwestern Pacific, respectively, indicating a northward shifted subtropical moisture transportation relative to the observation (Figure 4b). Consistently, the WPSH ridge in the CMIP6 MME is located northwards with respect to observations, especially around the western boundary of the WPSH (Figure 5). In addition, the southwesterlies (the tropical monsoon part) are
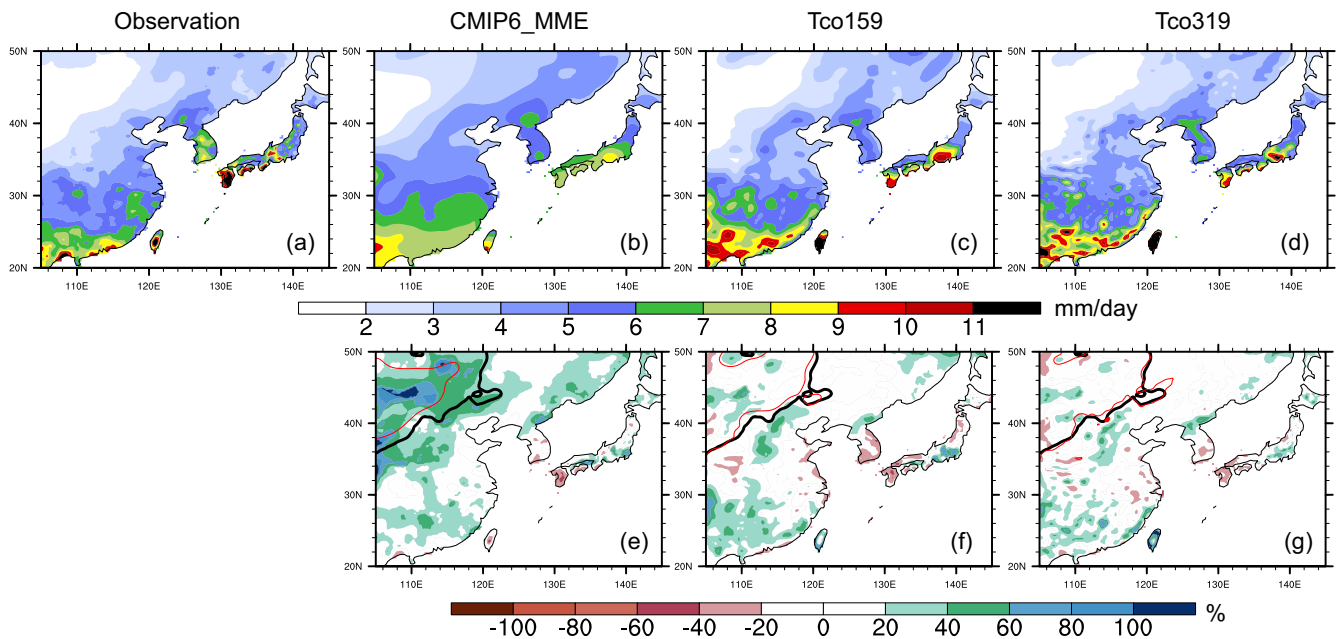
FIGURE 3 Climatological JJA precipitation over East Asia in APHRODITE (Observation), CMIP6 MME, as well as AWI-CM3 at TCo159 and TCo319 resolution (the first row, mm·day^{-1}). The second row shows the modelled JJA precipitation bias, shown as percentages relative to the observation, in corresponding climate models. Thin and thick contours depict the northern boundary of the EASM in observation and climate models, where the northern boundary is defined as the climatological 2 mm·day^{-1} isohyet averaged from May to September [Colour figure can be viewed at wileyonlinelibrary.com]

also overestimated, causing an overall increase in the EASM spanning from the tropical to extratropical region (Figure 4b). Coupled with the northerly anomalies with enhanced cold air, excessive precipitation occurs over the middle latitude of East Asia in the CMIP6 MME (Figure 3).

For AWI-CM3 with TCo159 resolution, the simulation shows an analogous bias in the subtropical lower-level winds to that of the CMIP6 MME (Figure 4c), indicating that both simulate an inaccurate WPSH. Nevertheless, the anomalous subtropical cyclone in AWI-CM3 is located further westward with respect to that simulated by the CMIP6 MME, extending to the Southeast Asian continent and causing a weakened EASM at low latitude. Therefore, there is an anomalous moisture convergence over south China, divergence over the Yangtze-Huai River region, South Korea and South Japan, and convergence over north China, corresponding to the meridional "more-less-more" precipitation bias over East Asia (Figure 3). Further analysis of the WPSH shows that the WPSH ridge in AWI-CM3 is located to the north of the observed WPSH ridge by approximately 5° of latitude (Figure 5). Moreover, the western boundary of WPSH also shows a notable retreat from the Asian continent compared to the observation and CMIP6 MME. Therefore, the northeastward shifted WPSH in AWI-CM3 has more impact on the East Asian precipitation in the north

of 35°N, while the WPSH in CMIP6 MME could affect the East Asian around 30°N (Figure 4c). The circulation bias pattern in AWI-CM3 with TCo319 is similar to that in TCo159 but with reduced amplitude (Figure 4d). The WPSH ridge in TCo319 is also closer to observation (Figure 5), which may be responsible for its improved precipitation performance compared to the TCo159.

The land–sea thermal contrast is the basis of EASM and, of course, the bias of summer EAP should be linked with the models' bias in tropospheric temperature. Here, we select 500–200 hPa averaged temperature to represent the tropospheric temperature as suggested by previous studies (Dai et al., 2013). In the summertime, the Asian continent is warmer than the adjacent ocean due to its lower heat capacity. Such land–sea thermal contrast is further enhanced by surface heating of the Tibetan Plateau, leading to a pressure gradient from the ocean to land that drives monsoon circulation (Figures 4a and 6). Although the CMIP6 MME simulates an overall cooling bias over the troposphere, it has a strong (weak) cooling over the extratropical (subtropical) North Pacific, inducing a higher (lower) pressure and consequently the anomalous anticyclone (cyclone) over there. In addition, the largest cooling bias at high latitudes implies more active cold air from the Arctic, corresponding to the overestimated northerlies (Figure 4b) accounting for the positive precipitation bias over middle-latitude Asia (Figure 3).
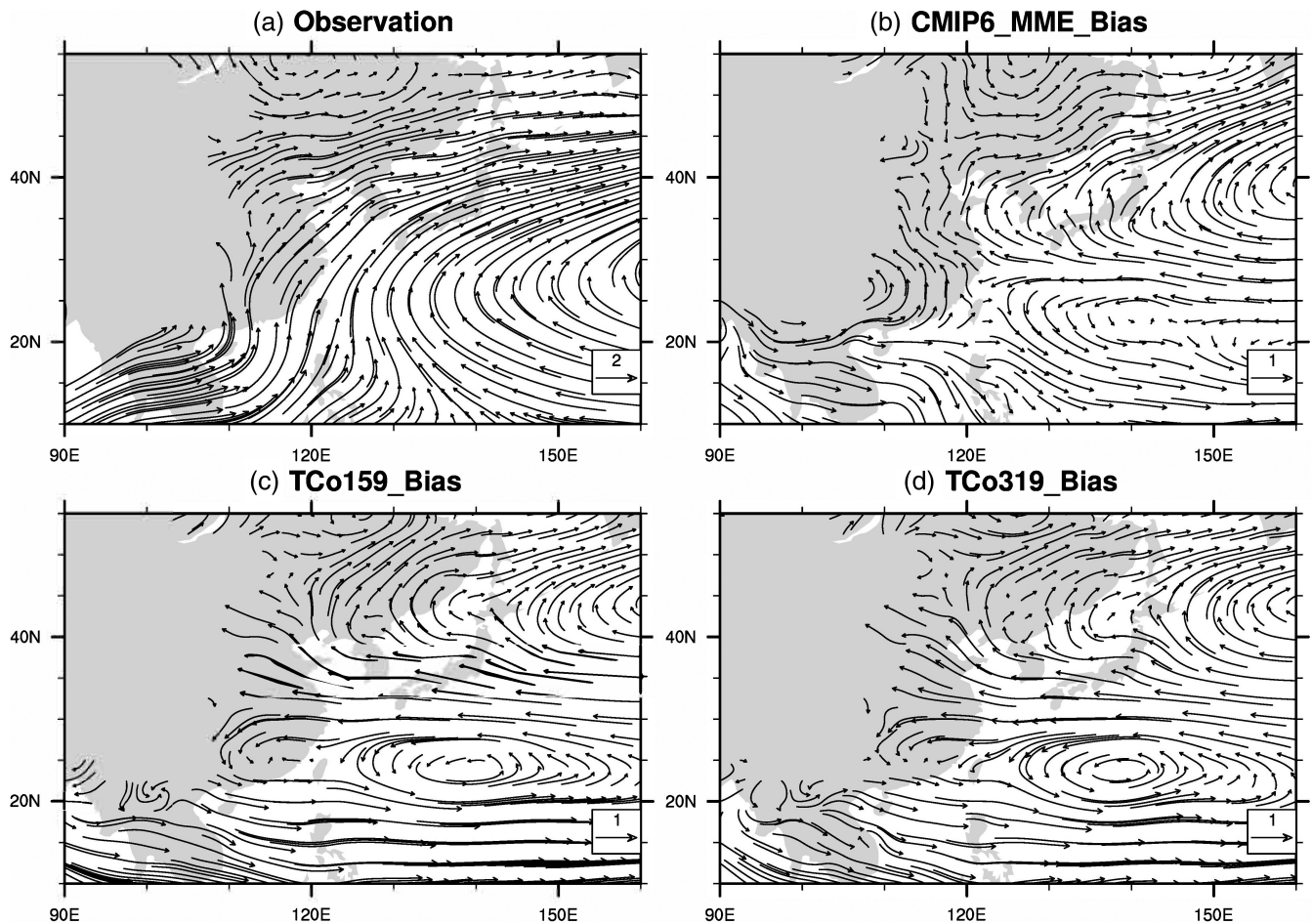
FIGURE 4 (a) Observed JJA 850 hPa winds in JRA-55. (b–d) Bias of modelled 850 hPa winds in the CMIP6 MME as well as in AWI-CM3 for TCo159 and TCo319 resolution, respectively. Units: m·s^{-1}

The tropospheric temperature in AWI-CM3 with TCo159 resolution, however, is generally warmer than the observation, distinct from the CMIP6 MME. The large warming biases over North Asia and the subtropical North Pacific correspond to the local lower pressure and anomalous cyclone, and the moderate warming over North Pacific creates a higher pressure (Figure 6) and anomalous anticyclone (Figure 4c). These thermal and pressure anomalies explain the monsoon circulation bias and the resulting precipitation bias (Figures 3). It is also found that the positive pressure bias over the North Pacific in AWI-CM3 is located much northeastward than that in CMIP6 MME, confirming their differences in the WPSH and lower-level winds bias, which is related to the sea surface temperature (SST) bias over the North Pacific: the colder SST in CMIP6 MME is located near the centre of North Pacific, while AWI-CM3's colder SST (relative to the surrounding ocean) is located further eastward (Figure 7). In addition, AWI-CM3 also simulates strong
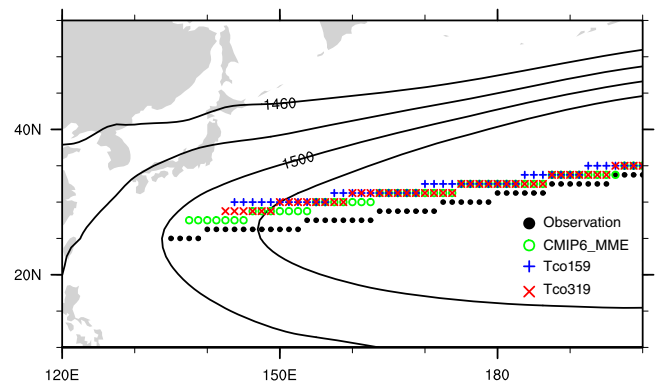

FIGURE 5 Observed summer 850 hPa geopotential height (contours, in geopotential meter, i.e., gpm) and the WPSH ridge in observation, CMIP6 MME, as well as AWI-CM3 at TCo159 and TCo319 resolution (scatters). The WPSH ridge is defined as the latitude of 850 hPa maximum geopotential height at each longitude. Areas with geopotential height larger than 1500 gpm are used to calculate the WPSH ridge [Colour figure can be viewed at wileyonlinelibrary.com]
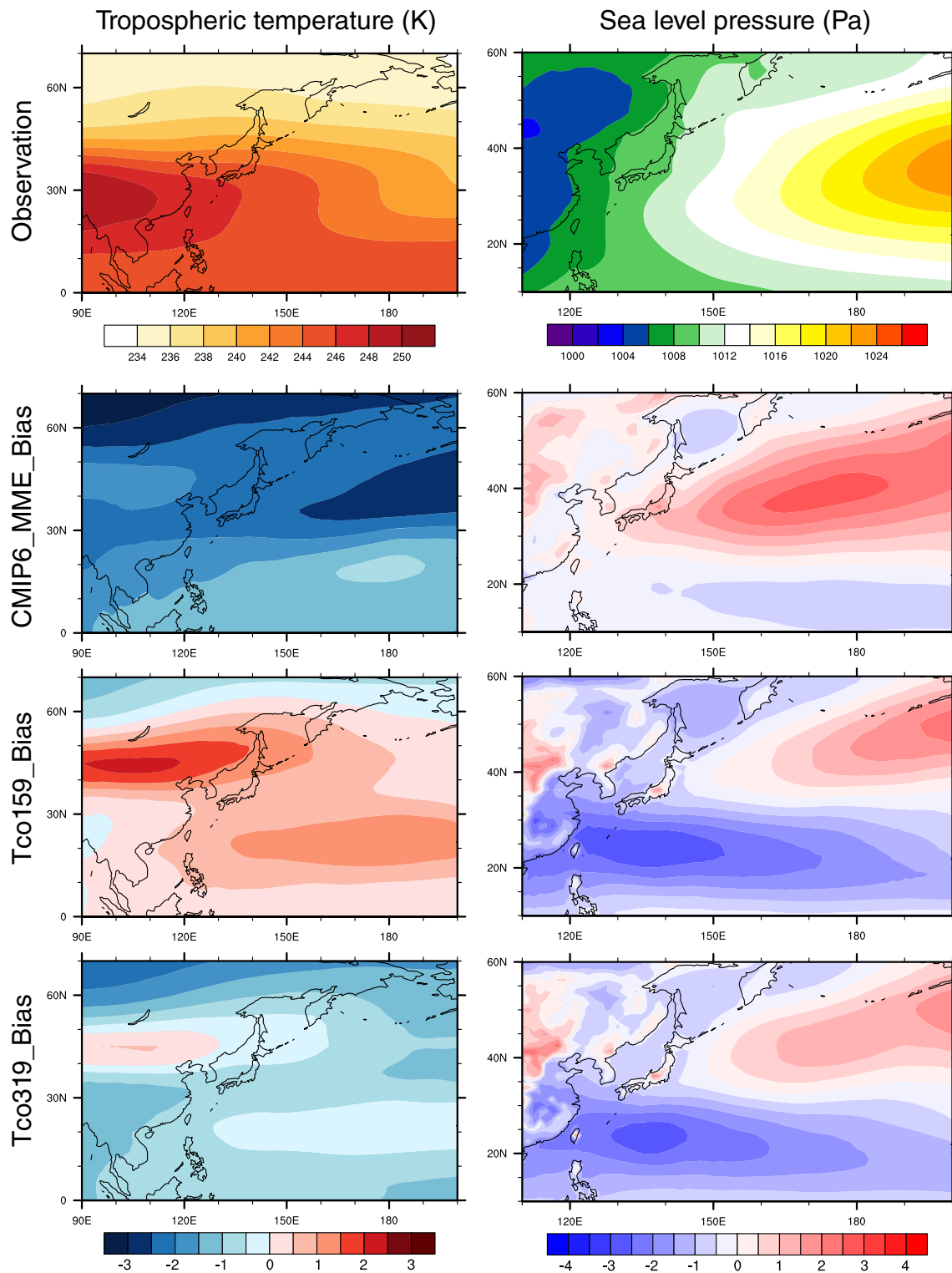
FIGURE 6 Summer tropospheric temperature (averaged from 500 to 200 hPa) in the observation, and their bias in the CMIP6 MME as well as in AWI-CM3 TCo159 and TCo319 (left column). Right column: as left column but for sea level pressure [Colour figure can be viewed at wileyonlinelibrary.com]

heating in the east of the maritime continent induced by the local warmer SST, resulting in a lower-level cyclonic circulation in its northwest direction (Figure 4c) according to the Gill-response (Gill, 1980). However, CMIP6 MME

produces a weaker warmer SST bias there and hence less impact on the atmospheric circulation.

For the AWI-CM3 simulation at TCo319 resolution, although its tropospheric temperature displays a cooling
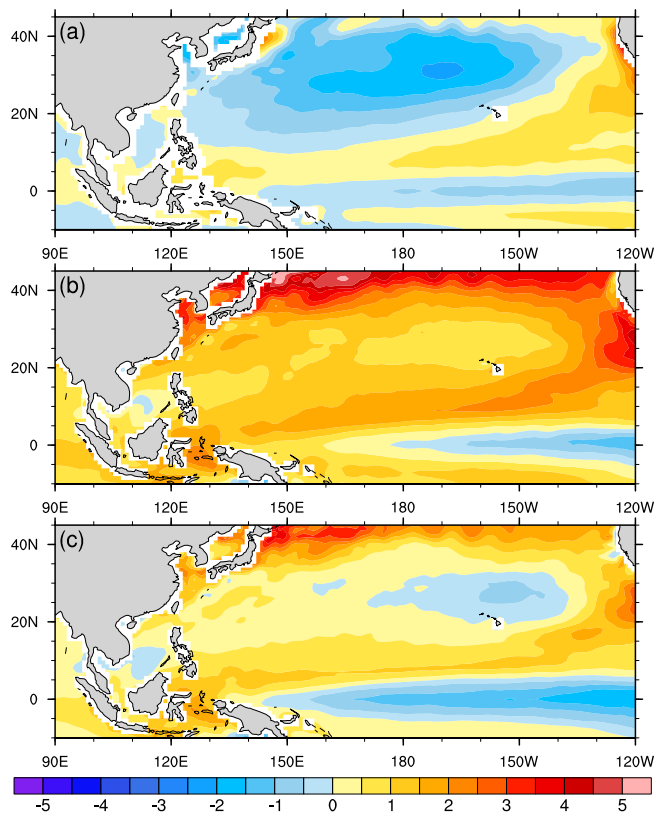
FIGURE 7 Bias of JJA SST in the (a) CMIP6 MME as well as in AWI-CM3 (b) TCo159 and (c) TCo319 relative to the observation. Unit: K [Colour figure can be viewed at wileyonlinelibrary.com]

bias over Asia and the Pacific, except for part of North Asia, its temperature contrast is quite analogous to that at TCo159 with a change of sign. As a result, the pressure bias of TCo319 also resembles that of TCo159 (Figure 6). It is noted that the amplitude of atmospheric temperature, pressure and SST bias in TCo319 are reduced, showing that increased atmosphere resolution improves model performance concerning summer circulation and precipitation in AWI-CM3 (Figures 3 and 4c,d).

4 | DECAYED SKILL OF EAP FROM JUNE TO AUGUST IN THE AWI-CM3
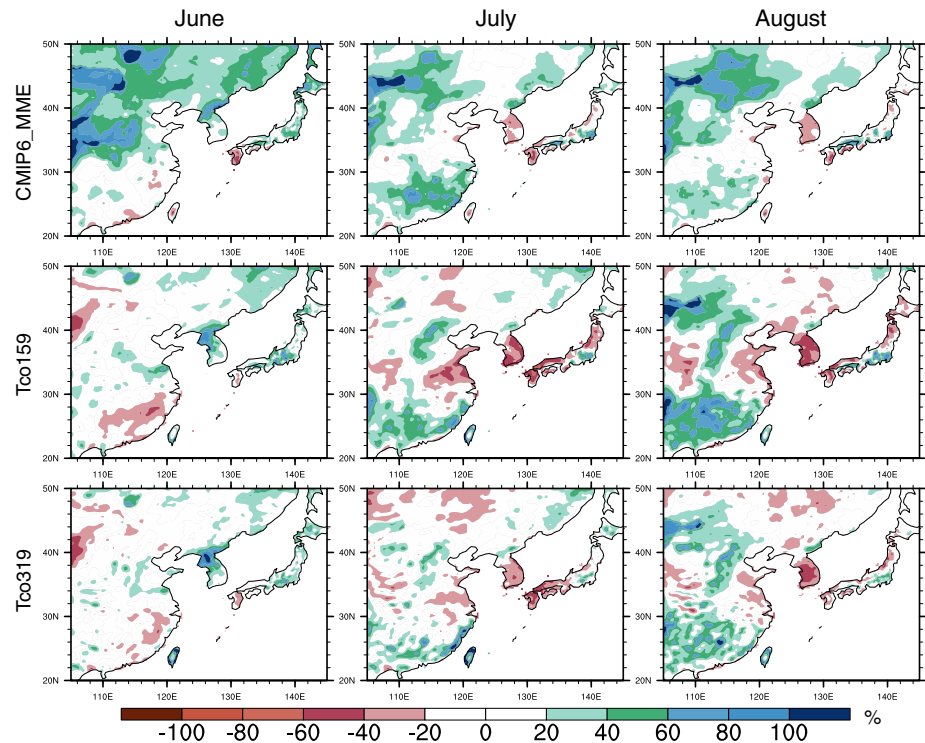
4.1 | Evaluation of AWI-CM3 and CMIP6 models

Despite the excellent skill of AWI-CM3 in reproducing the summer mean EAP, the performance of AWI-CM3 is modulated for individual months of the summer season. In June, the AWI-CM3 exhibits a high SCC close to the CMIP6 MME but shows a smaller bias regarding the NSD, implying a much better performance than the

CMIP6 MME evaluated by the skill scores (Figure 1b). In July and August, AWI-CM3 has NSDs similar to the CMIP6 MME, but with poor SCCs. Hence, AWI-CM3 has a lower skill in simulating local precipitation in late summer (Figure 1c,d). The TCo319 simulation has a higher SCC and a smaller NSD bias than the TCo159 simulation in all months and seasonal averages, showing an advantage in simulating the EAP when higher spatial resolution is considered in the atmosphere model.

Revealed by the models' skill scores, the AWI-CM3 with TCo319 resolution is comparable with the best individual CMIP6 model in the skill to simulate June precipitation over East Asia (Figure 2b). Although performance is relatively reduced at TCo159, AWI-CM3 still exhibits a higher skill score than the CMIP6 MME. The excellent performance of AWI-CM3 is ascribed to its reasonable reproduction of the standard deviation, which is the reasonable spatial variability, of June precipitation over East Asia (Figure 1b). In contrast, in July and August, the CMIP6 MME attains skill scores higher than approximated 90% and 80% models, respectively, better than AWI-CM3 at TCo159 and TCo319 (Figure 2c,d). Due to its mediocre SCC performance, AWI-CM3 at TCo319 resolution only shows scores better than about 80% and 70% CMIP6 models for July and August, respectively, which shows an obvious degraded model performance than for June. Yet, also for these months of relatively weaker performance, AWI-CM3 at TCo319 resolution still ranks among the top 1/3 of all CMIP6 models. Nevertheless, AWI-CM3 at TCo159 resolution gets a relatively low score especially in August, even falling behind half of the CMIP6 models, caused by its exaggerated NSD and poor SCC.

Specifically, a strong overestimation of precipitation is simulated by CMIP6 for north China and Mongolia throughout the summer season, similar to the season mean bias, with the largest bias occurring in June (Figure 8). Meanwhile, the CMIP6 MME exhibits a slight overestimation over South China of the summer precipitation, which mainly concentrates on July and August. For south China, AWI-CM3 simulates insufficient precipitation in June, and strongly overestimates observed precipitation in July and August, resulting in the impression that summer averaged precipitation has a similar deviation to that of the CMIP6 MME. In addition, AWI-CM3 also simulates less precipitation over the Yangtze-Huai River region, Korean Peninsula and South Japan in late summer. It is noteworthy that the precipitation bias in AWI-CM3 (both resolutions) exhibits a northward movement from June to August (Figure 8). For example, drought bias concentrates over South China in June, but shifts to the lower reaches of the Yangtze River and South Korea in July and moves to north China and the whole Korean Peninsula in August. This seasonal

FIGURE 8   Bias of modelled precipitation in CMIP6 MME as well as AWI-CM3 at TCo159 and TCo319 resolution in individual summer months, shown as percentages relative to APHRODITE [Colour figure can be viewed at wileyonlinelibrary.com]

movement of model bias is distinct from the CMIP6 MME results, which have exaggerated precipitation in north and south China throughout the summer months, implying different causes of the seasonal bias between AWI-CM3 and CMIP6 models.

4.2 | Causes of the decayed skill in AWI-CM3

As revealed before, the bias of WPSH and related atmospheric circulation in climate models play an important role in the summer precipitation bias over East Asia. As shown in Figure 9, the subtropical moisture sources along with the WPSH show a significant seasonal shift during summer. The WPSH and associated moisture transport move from the subtropical region in June to extratropical Asia in July and shift away from the continent in August, which is also clearly exhibited in the WPSH edge evolution (Figure 10) and causes the monthly movement of the precipitation maximum in the mid-latitudes. Meanwhile, the tropical monsoon features southerlies throughout the summertime, forming abundant precipitation over south China (Figure S7). For the CMIP6 MME, its monthly circulation bias is similar to the seasonal average (Figures 4a and 9). Due to the seasonal movement of WPSH (Figure 10), the WPSH bias in CMIP6 MME shifts northward as well during the summer (Figure 9). However, as the anomalous subtropical cyclone is located far away from the Asian continent, the

moisture transported to East Asia is mainly affected by the anomalous anticyclone over the extratropical North Pacific. Meanwhile, the cold air from high latitude areas also enhances throughout summer (Figure 9), hence more precipitation occurs over North Asia in all summer months in the CMIP6 MME (Figure 8).

In AWI-CM3, the monsoon circulation bias also experiences a similar northward movement with the WPSH (Figures 9 and 10). Nevertheless, as both the extratropical anomalous anticyclone and subtropical anomalous cyclone have impacts on the EAP, the precipitation bias pattern exhibits a seasonal movement as well (Figure 8). It is noted that, although CMIP6 MME and AWI-CM3 both stimulate excessive precipitation over North China in July and August, their mechanisms differ significantly. The WPSH ridge simulated by AWI-CM3, especially with TCo159 resolution, is located much north of that found in the observation, by 7° and 10° of latitude in July and August, respectively (Figure 10b,c). Therefore, the excessive precipitation over North China is caused by the overestimated moisture that is transported along the WPSH (Figure 9). The differences in 850 hPa winds between TCo319 and TCo159 simulations are almost opposite to the TCo159 bias, indicating better performance in the higher resolution simulation (Figure 9). In addition, although the simulation at TCo319 resolution has some improvements in simulating the WPSH ridge in comparison to the simulation performed at TCo159 resolution, it still shows considerable bias relative to the CMIP6 MME and observational data in late summer (Figure 10b,c).
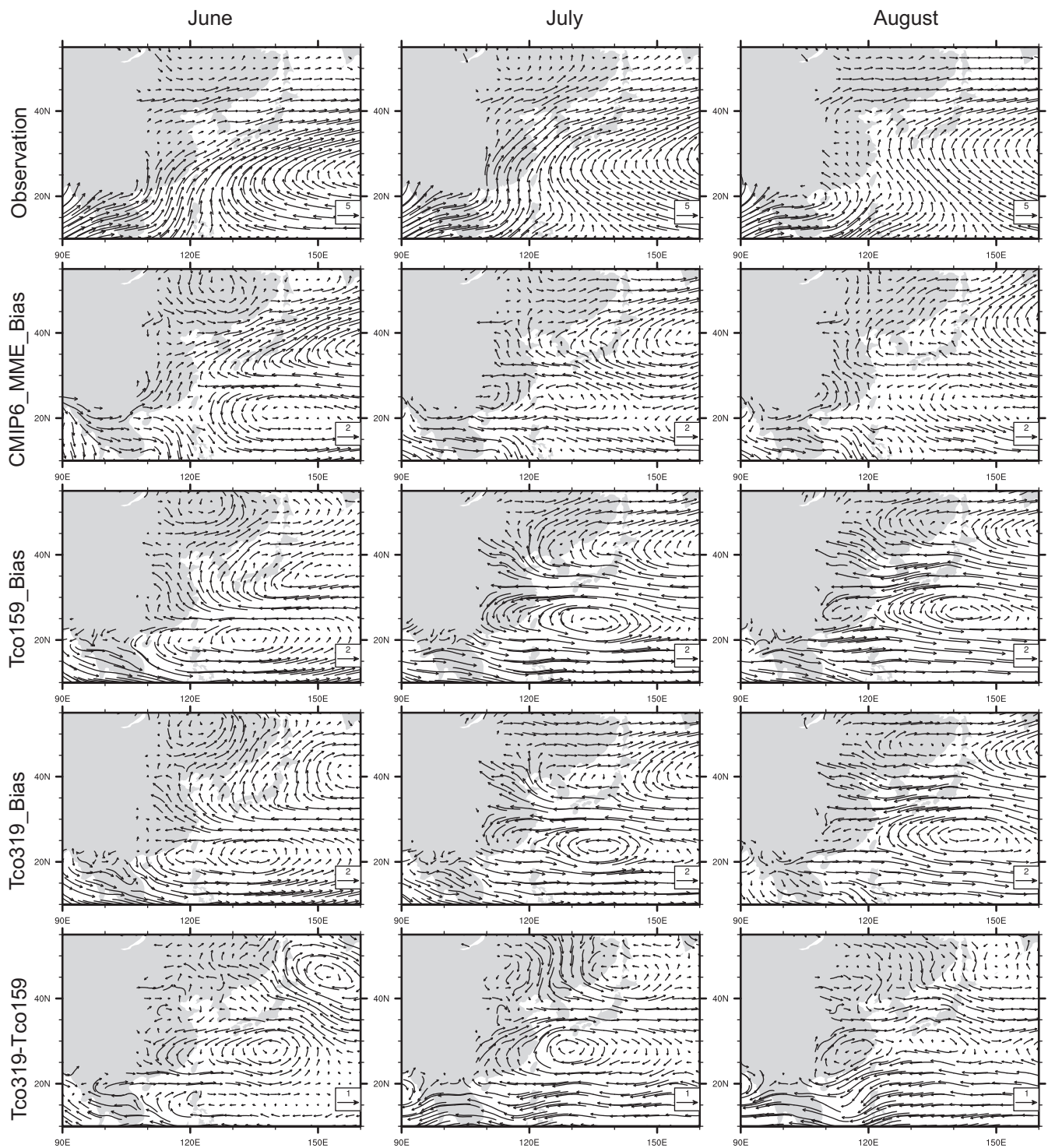
FIGURE 9 Climatological 850 hPa winds in JRA-55 for individual summer months (first row), and their bias in the CMIP6 MME as well as AWI-CM3 at TCo159 and TCo319 resolution (from the second to fourth rows), respectively. The fifth row is the difference between AWI-CM simulations at TCo319 and TCo159 resolutions, respectively. Units: m·s^{-1}

5 | SUMMARY AND CONCLUSIONS

We provide a thorough evaluation of AWI-CM3′s skill in simulating the summer precipitation over East Asia.

We compare results from two AWI-CM3 simulations performed with different atmospheric resolutions to see whether the resolution change could improve model performance. In order to facilitate a comparison of the AWI-CM3′s performance, we also evaluate the
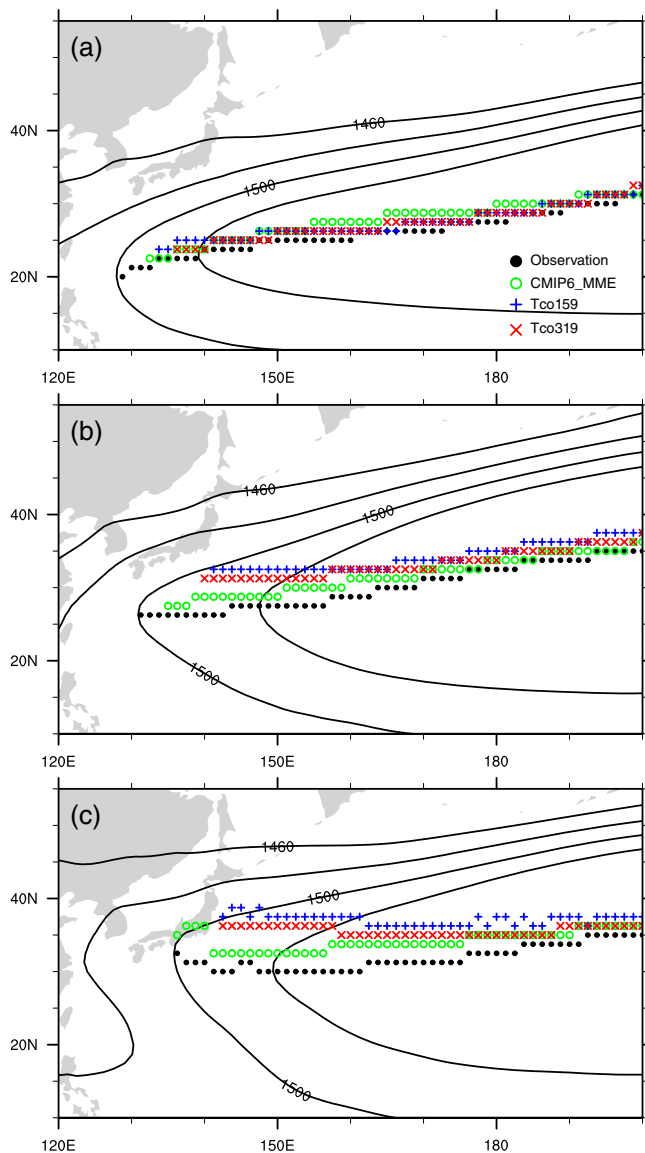
FIGURE 10 Same as Figure 5, except for (a) June, (b) July and (c) August, respectively [Colour figure can be viewed at wileyonlinelibrary.com]

CMIP6 models and compare results to those gained with the AWI-CM3.

Regarding the summer mean precipitation over East Asia, both AWI-CM3 simulations perform quite well in reproducing the observations—better than most individual CMIP6 models. The summer averaged EAP bias is concentrated over South China in AWI-CM3, caused by its underestimated low-latitude EASM and the northeastward shifted WPSH. In contrast, the CMIP6 MME produces an overall strengthening in the EASM and a northward-shifted WPSH, resulting in excessive precipitation over North China. These biases in EASM precipitation and circulation are dynamically linked to the discord of the large-scale thermal and pressure contrast in climate

models. Comparing the AWI-CM3 with CMIP6 models, we conclude that the atmospheric resolution of the climate models is quite important to the reproduction of East Asian summer precipitation. First, the summer precipitation over East Asia is mainly convective precipitation that corresponds to the local synoptic or climate system. Climate models without enough high atmosphere resolution could fail to reflect these small-scale systems. Gao et al. (2006) suggested that a 60 km resolution is necessary by testing different atmospheric resolutions in the same model. Therefore, both the AWI-CM3 simulations are able to produce precipitation-related small-scale systems, and the TCo319 performs better than TCo159. Second, the more detailed land orography in the atmosphere model with the finer resolution is favourable to the regional precipitation maximum, such as over the mountain areas (Figure 3). However, the typical atmospheric resolutions of CMIP6 models are coarser than 100 km, which is insufficient to resolve the precipitation that resulted from small-scale systems and local orography.

It is noted that the good reproduction of the EAP in AWI-CM3 in summer is mainly due to its excellent simulation of the June precipitation over East Asia, whose performance is comparable to the best CMIP6 individual models. However, AWI-CM3′s skill for EASM precipitation weakens progressively in July and August. Especially for the AWI-CM3 at a lower resolution, simulated EASM precipitation in August only outperforms less than 40% of the CMIP6 models. However, as the precipitation over East Asia mainly concentrates in June (Figure S7), the performance of summer mean precipitation in climate models is also dominated by their performance for June precipitation. Such a decayed skill of AWI-CM3 from June to August is closely related to the seasonal movement of the EASM circulation bias, particularly the WPSH. In June, the WPSH, as well as its bias, is located at low latitudes, thus introducing less impact on EASM precipitation. However, along with the poleward moved WPSH from June to August, the WPSH bias also shifts from low- to mid-latitude, producing more and more effect on the EASM precipitation bias. Therefore, more effort should be paid to improve the WPSH simulation in AWI-CM3. One possible reason is that the FESOM2 simulates a more over-extended climatological equatorial cold tongue than most CMIP6 models, although it is a common problem in climate models (Figure 7), which may result from the bias in the convection scheme (Song & Zhang, 2009), shortwave–SST feedback (Bayr et al., 2018) or evaporation–SST feedback (Zhang & Song, 2010). This cold tongue bias could affect the subtropical high through sea-air interaction, which then alters the precipitation over East Asia.

AWI-CM3 uses the OpenIFS as its new atmosphere module. Given the fact that the EC-Earth3 family using

the IFS (similar to OpenIFS but with data assimilation) also performs well among all CMIP6 models, the Open-IFS should be the main reason accounting for the improvement of AWI-CM3 relative to its predecessors participating in the CMIP6 (AWI-CM-1-1-MR and AWI-ESM-1-1-LR) who used the ECHAM6.3 as their atmosphere model. Some factors could affect our conclusions. Besides the uncertainty from the comparison between the equilibrium simulation and the transient observation and CMIP6 results, we could not run the high-resolution AWI-CM3 simulations for enough model years as the typical CMIP6 simulations to fully reach equilibrium states, which also induces uncertainties to this study. Despite those, Streffing et al. (2022) showed that the AWI-CM3 transient simulation with TCo159 already outperforms CMIP6 in many large-scale climatologies, and features above CMIP6-average skills. We here confirm this conclusion for specific aspects of more regional climate (i.e., the East Asian precipitation), although model setups different from those employed by Streffing et al. (2022) are applied. Furthermore, we conclude that employing AWI-CM3 at a higher spatial resolution of the atmosphere model indeed improves the simulation of the EAP. The TCo319 simulation surpasses the quality of the TCo159 simulation in all aspects taken into account (e.g., summer mean, monthly EAP, and precipitation-related atmospheric circulations and SST patterns), performing similar to, and even better than, the CMIP6 MME in many respects. It should be mentioned that although both of our AWI-CM3 simulations employ a higher resolution OpenIFS than typical CMIP6 models, the considerable computational efficiency of OpenIFS and FESOM2 makes it practicable to equilibrate the AWI-CM3 at an affordable computational expense. From this point of view, the AWI-CM3, in particular at TCo319 resolution, is suggested as a tool for investigating East Asian precipitation for past and future climates, where proxies or climate models still have large uncertainties.

AUTHOR CONTRIBUTIONS

Jian Shi: Conceptualization; writing – original draft; writing – review and editing; methodology; investigation; funding acquisition; visualization. **Christian Stepanek:** Writing – review and editing; funding acquisition; resources; validation. **Dmitry Sein:** Methodology; data curation; validation; funding acquisition. **Jan Streffing:** Data curation; validation; funding acquisition. **Gerrit Lohmann:** Supervision; funding acquisition; writing – review and editing; validation; resources.

ACKNOWLEDGEMENTS

ORCID
Jian Shi https://orcid.org/0000-0002-0703-4612

REFERENCES

Bayr, T., Latif, M., Dommenget, D., Wengel, C., Harlaß, J. & Park, W. (2018) Mean-state dependence of ENSO atmospheric feedbacks in climate models. *Climate Dynamics*, 50(9–10), 3171–3194. Available from: https://doi.org/10.1007/S00382-017-3799-2/FIGURES/16

Chen, H. & Sun, J. (2013) Projected change in East Asian summer monsoon precipitation under RCP scenario. *Meteorology and Atmospheric Physics*, 121(1–2), 55–77. Available from: https://doi.org/10.1007/s00703-013-0257-5

Chen, J., Zhang, Q., Huang, W., Lu, Z., Zhang, Z. & Chen, F. (2021) Northwestward shift of the northern boundary of the East Asian summer monsoon during the mid-Holocene caused by orbital forcing and vegetation feedbacks. *Quaternary Science Reviews*, 268, 107136. Available from: https://doi.org/10.1016/j.quascirev.2021.107136

Dai, A., Li, H., Sun, Y., Hong, L.C., Ho, L., Chou, C. et al. (2013) The relative roles of upper and lower tropospheric thermal contrasts and tropical influences in driving Asian summer monsoons. *Journal of Geophysical Research Atmospheres*, 118(13), 7024–7045. Available from: https://doi.org/10.1002/jgrd.50565

Danilov, S., Sidorenko, D., Wang, Q. & Jung, T. (2017) The finite-volumE sea ice–ocean model (FESOM2). *Geoscientific Model Development*, 10(2), 765–789.

Ding, T., Zhou, T., Chen, X., Zou, L., Li, P., Roberts, M.J. et al. (2021) Enhanced turbulent heat fluxes improve Meiyu-Baiu

simulation in high-resolution atmospheric models. *Journal of Advances in Modeling Earth Systems*, 13(9), e2020MS002430. Available from: https://doi.org/10.1029/2020MS002430

ECMWF. (2017a) *IFS documentation CY43R3—part III: dynamics and numerical procedures*. Reading, UK: ECMWF. Available from: https://doi.org/10.21957/8l7miod5m

ECMWF. (2017b) *IFS documentation CY43R3—part IV: physical processes*. Reading, UK: ECMWF. Available from: https://doi.org/10.21957/efyk72kl

ECMWF. (2017c) *IFS documentation CY43R3—part VII: ECMWF wave model*. Reading, UK: ECMWF. Available from: https://doi.org/10.21957/mxz9z1gb

Feng, J., Wei, T., Dong, W., Wu, Q. & Wang, Y. (2014) CMIP5/A-MIP GCM simulations of East Asian summer monsoon. *Advances in Atmospheric Sciences*, 31(4), 836–850. Available from: https://doi.org/10.1007/s00376-013-3131-y

Fu, J., Li, S. & Luo, D. (2009) Impact of global SST on decadal shift of East Asian summer climate. *Advances in Atmospheric Sciences*, 26(2), 192–201. Available from: https://doi.org/10.1007/s00376-009-0192-z

Gao, X., Shi, Y., Song, R., Giorgi, F., Wang, Y. & Zhang, D. (2008) Reduction of future monsoon precipitation over China: comparison between a high resolution RCM simulation and the driving GCM. *Meteorology and Atmospheric Physics*, 100(1–4), 73–86. Available from: https://doi.org/10.1007/s00703-008-0296-5

Gao, X., Xu, Y., Zhao, Z., Pal, J.S. & Giorgi, F. (2006) On the role of resolution and topography in the simulation of East Asia precipitation. *Theoretical and Applied Climatology*, 86(1–4), 173–185. Available from: https://doi.org/10.1007/s00704-005-0214-4

Gill, A.E. (1980) Some simple solutions for heat-induced tropical circulation. *Quarterly Journal of the Royal Meteorological Society*, 106(449), 447–462. Available from: https://doi.org/10.1002/QJ.49710644905

Hansen, J., Ruedy, R., Sato, M. & Lo, K. (2010) Globalsurface temperature change. *Reviews of Geophysics*, 48, RG4004.

Harris, I., Osborn, T.J., Jones, P. & Lister, D. (2020) Version 4 of the CRU TS monthly high-resolution gridded multivariate climate dataset. *Scientific Data*, 7(1), 1–18. Available from: https://doi.org/10.1038/s41597-020-0453-3

Haywood, A.M., Tindall, J.C., Dowsett, H.J., Dolan, A.M., Foley, K. M., Hunter, S.J. et al. (2020) The Pliocene model Intercomparison Project phase 2: large-scale climate features and climate sensitivity. *Climate of the Past*, 16(6), 2095–2123. Available from: https://doi.org/10.5194/cp-16-2095-2020

Huang, D.Q., Zhu, J., Zhang, Y.C. & Huang, A.N. (2013) Uncertainties on the simulated summer precipitation over eastern China from the CMIP5 models. *Journal of Geophysical Research: Atmospheres*, 118(16), 9035–9047. Available from: https://doi.org/10.1002/jgrd.50695

Jiang, D., Hu, D., Tian, Z. & Lang, X. (2020) Differences between CMIP6 and CMIP5 models in simulating climate over China and the East Asian monsoon. *Advances in Atmospheric Sciences*, 37(10), 1102–1118. Available from: https://doi.org/10.1007/s00376-020-2034-y

Jiang, D., Tian, Z. & Lang, X. (2016) Reliability of climate models for China through the IPCC third to fifth assessment reports. *International Journal of Climatology*, 36(3), 1114–1133. Available from: https://doi.org/10.1002/joc.4406

Jung, T., Gulev, S.K., Rudeva, I. & Soloviov, V. (2006) Sensitivity of extratropical cyclone characteristics to horizontal resolution in the ECMWF model. *Quarterly Journal of the Royal Meteorological Society*, 132(619), 1839–1857. Available from: https://doi.org/10.1256/qj.05.212

Kobayashi, S., Ota, Y., Harada, Y., Ebita, A., Moriya, M., Onoda, H. et al. (2015) The JRA-55 reanalysis: general specifications and basic characteristics. *Journal of the Meteorological Society of Japan*, 93(1), 5–48. Available from: https://doi.org/10.2151/jmsj.2015-001

Lei, Y., Hoskins, B. & Slingo, J. (2011) Exploring the interplay between natural decadal variability and anthropogenic climate change in summer rainfall over China. Part I: observational evidence. *Journal of Climate*, 24(17), 4584–4599. Available from: https://doi.org/10.1175/2010JCLI3794.1

Li, H., Dai, A., Zhou, T. & Lu, J. (2010) Responses of East Asian summer monsoon to historical SST and atmospheric forcing during 1950–2000. *Climate Dynamics*, 34(4), 501–514. Available from: https://doi.org/10.1007/s00382-008-0482-7

Li, Z., Sun, Y., Li, T., Ding, Y. & Hu, T. (2019) Future changes in East Asian summer monsoon circulation and precipitation under 1.5 to 5°C of warming. *Earth's Futures*, 7(12), 1391–1406. Available from: https://doi.org/10.1029/2019EF001276

Lin, R., Zhu, J. & Zheng, F. (2016) Decadal shifts of East Asian summer monsoon in a climate model free of explicit GHGs and aerosols. *Scientific Reports*, 6(1), 1–9. Available from: https://doi.org/10.1038/srep38546

Lohmann, G., Wagner, A. & Prange, M. (2021) Resolution of the atmospheric model matters for the Northern Hemisphere mid-Holocene climate. *Dynamics of Atmospheres and Oceans*, 93, 101206. Available from: https://doi.org/10.1016/j.dynatmoce.2021.101206

Piao, J., Chen, W., Wang, L., Pausata, F.S.R. & Zhang, Q. (2020) Northward extension of the East Asian summer monsoon during the mid-Holocene. *Global and Planetary Change*, 184, 103046. Available from: https://doi.org/10.1016/j.gloplacha.2019.103046

Potter, G.L. (1995) *The effect of horizontal resolution on cloud radiative forcing in the ECMWF model*. Livermore, CA: Lawrence Livermore National Lab. (LLNL). PCMDI report no. 22.

Rayner, N.A., Parker, D.E., Horton, E.B., Folland, C.K., Alexander, L.V., Rowell, D.P. et al. (2003) Global analyses of sea surface temperature, sea ice, and night marine air temperature since the late nineteenth century. *Journal of Geophysical Research: Atmospheres*, 108(D14), 4407. Available from: https://doi.org/10.1029/2002JD002670

Schneider, U., Hänsel, S., Finger, P., Rustemeier, E. & Ziese, M. (2022) *GPCC Full Data Monthly Product version 2022 at 0.25°: monthly land-surface precipitation from rain-gauges built on GTS-based and historical data*. Global Precipitation Climatology Centre at Deutscher Wetterdienst. Available from: https://opendata.dwd.de/climate_environment/GPCC/html/fulldata-monthly_v2022_doi_download.html

Sein, D.V., Danilov, S., Biastoch, A., Durgadoo, J.V., Sidorenko, D., Harig, S. et al. (2016) Designing variable ocean model resolution based on the observed ocean variability. *Journal of Advances in Modeling Earth Systems*, 8(2), 904–916. Available from: https://doi.org/10.1002/2016MS000650

Seo, K.H., Ok, J., Son, J.H. & Cha, D.H. (2013) Assessing future changes in the East Asian summer monsoon using CMIP5

coupled models. *Journal of Climate*, 26(19), 7662–7675. Available from: https://doi.org/10.1175/JCLI-D-12-00694.1

Song, F. & Zhou, T. (2014) Interannual variability of East Asian summer monsoon simulated by CMIP3 and CMIP5 AGCMs: skill dependence on Indian Ocean-western pacific anticyclone teleconnection. *Journal of Climate*, 27(4), 1679–1697. Available from: https://doi.org/10.1175/JCLI-D-13-00248.1

Song, X. & Zhang, G.J. (2009) Convection parameterization, tropical Pacific double ITCZ, and upper-ocean biases in the NCAR CCSM3. Part I: climatology and atmospheric feedback. *Journal of Climate*, 22(16), 4299–4315. Available from: https://doi.org/10.1175/2009JCLI2642.1

Streffing, J., Sidorenko, D., Semmler, T., Zampieri, L., Scholz, P., Andrés-Martínez, M. et al. (2022) AWI-CM3 coupled climate model: description and evaluation experiments for a prototype post-CMIP6 model. *Geoscientific Model Development*, 15(16), 6399–6427. Available from: https://doi.org/10.5194/GMD-15-6399-2022

Taylor, K.E. (2001) Summarizing multiple aspects of model performance in a single diagram. *Journal of Geophysical Research: Atmospheres*, 106(D7), 7183–7192. Available from: https://doi.org/10.1029/2000JD900719

Tian, F., Dong, B., Robson, J. & Sutton, R. (2018) Forced decadal changes in the East Asian summer monsoon: the roles of greenhouse gases and anthropogenic aerosols. *Climate Dynamics*, 51(9–10), 3699–3715. Available from: https://doi.org/10.1007/s00382-018-4105-7

Tian, Z. & Jiang, D. (2013) Mid-Holocene ocean and vegetation feedbacks over East Asia. *Climate of the Past*, 9(5), 2153–2171. Available from: https://doi.org/10.5194/cp-9-2153-2013

Tibaldi, S., Palmer, T.N., Branković, C. & Cubasch, U. (1990) Extended-range predictions with ECMWF models: influence of horizontal resolution on systematic error and forecast skill. *Quarterly Journal of the Royal Meteorological Society*, 116(494), 835–866. Available from: https://doi.org/10.1002/qj.49711649404

Wang, B., Liu, J., Kim, H.J., Webster, P.J. & Yim, S.Y. (2012) Recent change of the global monsoon precipitation (1979-2008). *Climate Dynamics*, 39, 1123–1135.

Wang, T., Wang, H.J., Otterå, O.H., Gao, Y.Q., Suo, L.L., Furevik, T. et al. (2013) Anthropogenic agent implicated as a prime driver of shift in precipitation in eastern China in the late 1970s. *Atmospheric Chemistry and Physics*, 13(24), 12433–12450. Available from: https://doi.org/10.5194/acp-13-12433-2013

Xin, X., Wu, T., Jie, W. & Zhang, J. (2021) Impact of higher resolution on precipitation over China in CMIP6 HighResMIP models. *Atmosphere*, 12(6), 762. Available from: https://doi.org/10.3390/atmos12060762

Xin, X., Wu, T., Zhang, J., Yao, J. & Fang, Y. (2020) Comparison of CMIP6 and CMIP5 simulations of precipitation in China and the East Asian summer monsoon. *International Journal of Climatology*, 40(15), 6423–6440. Available from: https://doi.org/10.1002/joc.6590

Yao, J., Zhou, T., Guo, Z., Chen, X., Zou, L. & Sun, Y. (2017) Improved performance of high-resolution atmospheric models in simulating the East Asian summer monsoon rain belt. *Journal of Climate*, 30(21), 8825–8840. Available from: https://doi.org/10.1175/JCLI-D-16-0372.1

Yatagai, A., Arakawa, O., Kamiguchi, K., Kawamoto, H., Nodzu, M. I. & Hamada, A. (2009) A 44-year daily gridded precipitation dataset for Asia based on a dense network of rain gauges. *Scientific Online Letters on the Atmosphere*, 5(1), 137–140. Available from: https://doi.org/10.2151/sola.2009-035

Yu, L., Furevik, T., Otterå, O.H. & Gao, Y. (2015) Modulation of the Pacific Decadal Oscillation on the summer precipitation over East China: a comparison of observations to 600-years control run of Bergen climate model. *Climate Dynamics*, 44(1–2), 475–494. Available from: https://doi.org/10.1007/s00382-014-2141-5

Zhang, G.J. & Song, X. (2010) Convection parameterization, tropical Pacific double ITCZ, and upper-ocean biases in the NCAR CCSM3. Part II: coupled feedback and the role of ocean heat transport. *Journal of Climate*, 23(3), 800–812. Available from: https://doi.org/10.1175/2009JCLI3109.1

Zheng, W., Wu, B., He, J. & Yu, Y. (2013) The East Asian summer monsoon at mid-Holocene: results from PMIP3 simulations. *Climate of the Past*, 9(1), 453–466. Available from: https://doi.org/10.5194/cp-9-453-2013

Zhou, S., Huang, G. & Huang, P. (2018) Changes in the East Asian summer monsoon rainfall under global warming: moisture budget decompositions and the sources of uncertainty. *Climate Dynamics*, 51(4), 1363–1373. Available from: https://doi.org/10.1007/s00382-017-3959-4

Zhu, C., Wang, B., Qian, W. & Zhang, B. (2012) Recent weakening of northern East Asian summer monsoon: a possible response to global warming. *Geophysical Research Letters*, 39(9), L09701. Available from: https://doi.org/10.1029/2012GL051155

SUPPORTING INFORMATION

Additional supporting information can be found online in the Supporting Information section at the end of this article.